Effects of electron-hole interaction on the dynamic structure factor: Application to nonresonant inelastic x-ray scattering

J. A. Soininen
Department of Physics, POB 9, FIN-00014, University of Helsinki, Finland

Eric L. Shirley
Optical Technology Division, Physics Laboratory, National Institute of Standards and Technology, Gaithersburg, Maryland 20899
(Received 24 January 2000)

We present a first-principles scheme for calculating the dynamic structure factor for conventional semiconductors and insulators. The dynamic structure factor relates closely to the inelastic x-ray scattering double-differential cross section for valence electrons, an application that we consider, but it is also probed using other techniques, such as electron energy-loss spectroscopy. In the present scheme the electron-hole interaction is taken into account. Theoretical results are compared with nonresonant inelastic x-ray scattering results for LiF, diamond, and wurtzite GaN. We show the importance of including the electron-hole interaction. Some other properties of an electron-hole pair in these materials are also studied.

I. INTRODUCTION

Inelastic x-ray scattering can be used to probe the dynamical properties of materials such as the electron excitations that are considered in this paper. In order to interpret the inelastic x-ray scattering results, it is important to model the scattering event as accurately as possible. The constituents of such a model in the case of crystalline materials are the information on its ground state prior to the scattering event and information about the excited states of the system after the x-ray photon has interacted with it. The ground-state properties of materials such as the electron density and band structure are relatively well known and can be quite well predicted from first-principles calculations. The results from mean-field theories, like the local-density approximation (LDA),[1] for the electron density and other structural properties have been found to be more than adequate. To get accurate values for band energies more elaborate theories such as the *GW* (Refs. 2 and 3) approximation can be used.

When an inelastic x-ray scattering event occurs, an electron-hole pair can be created. How the electron and hole in such an excited state interact with each other and the surrounding electrons is probed by a scattering experiment. There have been several experiments[4] highlighting this property of inelastic scattering. Also several first-principles schemes have been previously suggested for calculating the dynamic structure factor.[5] The excited electron interacts with the hole, the polarization cloud produced by the hole, and its own polarization cloud. All these interactions are accounted for in this paper. However, we restrict our study to zero temperature, and the crystal is considered to be static. Essentially, the method used here is an extension of the one used for calculating ordinary optical absorption spectra.[6] Meanwhile, we note that the theoretical methods used here can also be applied to other techniques in addition to inelastic x-ray scattering, such as electron energy-loss spectroscopy.

The rest of the paper is structured as follows. In the following section, we describe how to use an effective Hamiltonian to introduce electron-hole interactions into the description of inelastic x-ray scattering and the dynamic structure factor. Next we review the properties of the Hamiltonian and some details of the numerical method. The study of the dynamic structure factor and inelastic x-ray scattering cross sections for LiF, diamond, and wurtzite GaN follows. Lastly we draw some conclusions.

II. INELASTIC X-RAY SCATTERING

The double differential cross section of inelastic x-ray scattering (IXS) can be written as

$$\frac{d^2\sigma}{d\Omega d\omega} = (d\sigma/d\Omega)_{Th} \sum_F |\langle F| \sum_i e^{i\mathbf{q}\cdot\mathbf{r}_i} |I\rangle|^2 \delta(E_F - E_I - \omega) \tag{1}$$

$$= (d\sigma/d\Omega)_{Th} S(\mathbf{q},\omega), \tag{2}$$

where $\mathbf{q}$ and ω are the momentum and energy transfer from the photon to the electrons of the system. The I (F) and E_I (E_F) denote initial (final) states and energies. We have used the Thompson cross section, $(d\sigma/d\Omega)_{Th} = r_0^2 |\boldsymbol{\epsilon}_1 \cdot \boldsymbol{\epsilon}_2|^2 \omega_2/\omega_1$, where r_0 is the classical electron radius. The polarization of the initial (final) photon is $\boldsymbol{\epsilon}_1$ ($\boldsymbol{\epsilon}_2$), and ω_1 (ω_2) is the photon energy. By changing the momentum and energy transfer one can determine the kinds of excitations produced in the sample. For solids, the low-momentum and energy-transfer region of the dynamic structure factor $S(\mathbf{q},\omega)$ is dominated by valence electron excitations.

In IXS, the photon can be seen as an external perturbing potential. Within linear-response theory, the macroscopic dielectric function of the system can be written as

$$\varepsilon_M(\mathbf{q},\omega) = 1 - \frac{4\pi}{q^2} \langle 0| \hat{\rho}_{\mathbf{q}} \frac{1}{\omega - \hat{H}_{eff} + i\eta} \hat{\rho}_{\mathbf{q}}^{\dagger} |0\rangle. \tag{3}$$

The macroscopic dielectric function ε_M, involves the response of the system to the total macroscopic field. $\hat{H}_{eff}$ is an effective Hamiltonian, $|0\rangle$ is the electronic ground state,

and $\rho_{\mathbf{q}}^{\dagger}$ is the density-fluctuation operator. The effective Hamiltonian is determined from the Bethe-Salpeter equation and level of approximation used. From the macroscopic dielectric function one obtains the dynamic structure factor via the fluctuation dissipation theorem using

$$S(\mathbf{q},\omega)=\frac{-q^2}{4\pi^2 n}\mathrm{Im}[1/\varepsilon_M(\mathbf{q},\omega)].$$

Here n is the average electron density in the solid.

III. METHOD DETAILS

In principle, calculating ε_M would require solution of the equations-of-motion (EOM) for the electron-hole pair operator, with a typical equation being

$$\langle\Phi|[\hat{H},\hat{a}_c^{\dagger}\hat{a}_v]|0\rangle=E\langle\Phi|\hat{a}_c^{\dagger}\hat{a}_v|0\rangle. \tag{4}$$

Here $\hat{H}$ is the exact Hamiltonian of the many-body system, $\hat{a}_c^{\dagger}\hat{a}_v$ is an electron-hole pair creation operator, and $|\Phi\rangle$ is an exact excited state with energy E. For computational reasons, one is forced to limit the types of excitations that are allowed in $|\Phi\rangle$. We choose to expand $|\Phi\rangle$ in terms of singly excited states, and in the ground state only the valence bands are occupied. This means that we are using the Tamm-Dancoff approximation (TDA).[7] Using these approximations we can extract an effective Hamiltonian H_{eff} from the EOM. For the rest of this section we briefly review the computational details of the scheme. A more detailed review can be found in Refs. 6 and 8.

A. Electron-hole pair wave function

Within the TDA an electron-hole pair wave function can be expanded in terms of single-particle wave functions:

$$\Psi_{\mathbf{q}}(\mathbf{r}_e,\mathbf{r}_h)=\sum_{vc\mathbf{k}} C_{vc\mathbf{k}}\psi_{v\mathbf{k}}^{*}(\mathbf{r}_h)\psi_{c\mathbf{k}+\mathbf{q}}(\mathbf{r}_e)\doteq\sum_{vc\mathbf{k}} C_{vc\mathbf{k}}|vc\mathbf{k}\rangle_{\mathbf{q}}.$$

Here $\mathbf{r}_e$ and $\mathbf{r}_h$ are the electron and hole coordinates, respectively. The hole is taken to be in a state with band index v and crystal momentum $\mathbf{k}$. The c is the electron state band index, and the electron has crystal momentum $\mathbf{k}+\mathbf{q}$. Because we work at the TDA level, the electron states are unoccupied in the ground state and the hole states are occupied. In practice this means that we allow only one electron-hole pair to exist at any given time. The single-particle wave functions $\psi_{i\mathbf{k}}(\mathbf{r})=u_{i\mathbf{k}}(\mathbf{r})\exp(i\mathbf{k}\cdot\mathbf{r})$ were taken from LDA pseudopotential[9] calculations. The periodic part u of the Bloch function was calculated using the optimized basis set of Ref. 10.

B. Effective Hamiltonian

The effective Hamiltonian to be used here can be written as

$$H_{eff}=H_e+H_h+H_{e-h}-\frac{4\pi}{q^2}\hat{\rho}_{\mathbf{q}}^{\dagger}\hat{\rho}_{\mathbf{q}}.$$

There is a single-particle part H_e+H_h, and electron-hole interaction term H_{e-h}. The term $(4\pi/q^2)\hat{\rho}_{\mathbf{q}}^{\dagger}\hat{\rho}_{\mathbf{q}}$ is subtracted because ε_M involves the response to the total (as opposed to external) macroscopic field. The electron-hole interaction contains a direct part ($\hat{V}_d$), with

$$\begin{aligned}{}_{\mathbf{q}}\langle vc\mathbf{k}|\hat{V}_d|v'c'\mathbf{k}'\rangle_{\mathbf{q}}=\sum_{\mathbf{R}}\int d\mathbf{x}d\mathbf{y}e^{i(\mathbf{k}'-\mathbf{k})\cdot(\mathbf{x}-\mathbf{y}+\mathbf{R})}\\ \times u_{c,\mathbf{k}+\mathbf{q}}^{*}(\mathbf{x})u_{v,\mathbf{k}}(\mathbf{y})W(\mathbf{x}+\mathbf{R},\mathbf{y})\\ \times u_{c',\mathbf{k}'+\mathbf{q}}(\mathbf{x})u_{v',\mathbf{k}'}^{*}(\mathbf{y}),\end{aligned} \tag{5}$$

and an exchange interaction ($\hat{V}_x$), with

$$\begin{aligned}{}_{\mathbf{q}}\langle vc\mathbf{k}|\hat{V}_x|v'c'\mathbf{k}'\rangle_{\mathbf{q}}=\sum_{\mathbf{R}}\int d\mathbf{x}d\mathbf{y}e^{-i\mathbf{q}\cdot(\mathbf{x}-\mathbf{y}+\mathbf{R})}\\ \times u_{c,\mathbf{k}+\mathbf{q}}^{*}(\mathbf{x})u_{v,\mathbf{k}}(\mathbf{x})V(\mathbf{x}+\mathbf{R},\mathbf{y})\\ \times u_{c',\mathbf{k}'+\mathbf{q}}(\mathbf{y})u_{v',\mathbf{k}'}^{*}(\mathbf{y}).\end{aligned} \tag{6}$$

In these equations $\mathbf{x}$ and $\mathbf{y}$ are vectors reduced to their respective unit cells of the crystal, and $\mathbf{R}$ connects these two unit cells. The function V in the exchange interaction is bare Coulomb interaction. The function W in the exchange term is the statically screened Coulomb interaction, so our effective Hamiltonian is Hermitian.

C. Haydock recursion solution

Inversion of the matrix $(\omega-\hat{H}_{eff}+i\eta)$ is computationally the most challenging part of the calculation of ε_M. The size of the matrix is determined by the number of two-particle states used in the calculations. In solid-state applications this number is large, and iterative methods are best suited for this problem. We use the Haydock recursion method.[11] There, a Hermitian Hamiltonian is reduced to tridiagonal form by starting from a normalized vector $|v_0\rangle$:

$$H|v_0\rangle=a_0|v_0\rangle+b_1|v_1\rangle, \tag{7}$$

$$H|v_1\rangle=b_1|v_0\rangle+a_1|v_1\rangle+b_2|v_2\rangle, \tag{8}$$

$$H|v_2\rangle=b_2|v_1\rangle+a_2|v_2\rangle+b_3|v_3\rangle,\ \text{etc.} \tag{9}$$

The real coefficients $\{a_i\}$ and $\{b_i\}$ can be chosen so that the resulting set of vectors $\{|v_i\rangle\}$ are orthonormal. By choosing the initial vector as $|v_0\rangle\propto\hat{\rho}_{\mathbf{q}}^{\dagger}|0\rangle$, we can calculate ε_M in continued fraction form (N for normalization)

$$\varepsilon_M(\mathbf{q},\omega)$$

$$=1-\frac{4\pi N}{q^2}\langle v_0|\frac{1}{\omega-\hat{H}_{eff}+i\eta}|v_0\rangle \tag{10}$$

$$=1-\frac{4\pi N}{q^2}\mathrm{Im}\left(\frac{1}{\omega+i\eta-a_0-b_1^2/(\omega+i\eta-a_1-\ldots)}\right). \tag{11}$$

We have found the Haydock recursion method to be a computationally efficient way of calculating ε_M. There is no need to repeat the recursion for each value of energy ω. Only four state vectors at each iteration step are needed, so the

memory requirements of this method are extremely small. The only requirements are that the Hamiltonian is Hermitian and that one can operate on a state vector.

D. Operating with the Hamiltonian

The single-particle part of the Hamiltonian is diagonal in the $|vc\mathbf{k}\rangle_{\mathbf{q}}$ basis, so operating with it on a particle-hole state simply multiplies it by the difference between the band energies of the hole and electron states:

$$(H_e+H_h)\sum_{vc\mathbf{k}} C_{vc\mathbf{k}}|vc\mathbf{k}\rangle_{\mathbf{q}}=\sum_{vc\mathbf{k}} C_{vc\mathbf{k}}(\epsilon^{GW}_{c,\mathbf{k}+\mathbf{q}}-\epsilon^{GW}_{v,\mathbf{k}})|vc\mathbf{k}\rangle_{\mathbf{q}}.$$

The band energies $\epsilon^{GW}_{c,\mathbf{k}+\mathbf{q}}$ and $\epsilon^{GW}_{v,\mathbf{k}}$ are corrected to agree with the calculated *GW* band energies when necessary. One might question the combined use of LDA single-particle wave functions and *GW* quasiparticle energies. In the cases studied here, however, LDA wave functions have been found to be close to the ones obtained from *GW* calculations.

$\hat{V}_x$ introduces ''local-field'' effects into ε_M because of induced microscopic electric fields at the unit-cell scale. Subtracting the term $(4\pi/q^2)\hat{\rho}^{\dagger}_{\mathbf{q}}\hat{\rho}_{\mathbf{q}}$ exactly cancels an identical term in $\hat{V}_x$ and we denote this $[\hat{V}_x-(4\pi/q^2)\hat{\rho}^{\dagger}_{\mathbf{q}}\hat{\rho}_{\mathbf{q}}]$ interaction by $\tilde{V}_x$. We operate on a state vector with $\tilde{V}_x$ in reciprocal space,

$$\tilde{V}_x\sum_{vc\mathbf{k}} C_{vc\mathbf{k}}|vc\mathbf{k}\rangle_{\mathbf{q}}=2\sum_{v'c'\mathbf{k}'}\left\{\sum_{\mathbf{G}\neq\mathbf{0}}\frac{4\pi}{\Omega|\mathbf{q}+\mathbf{G}|^2}\rho_{\mathbf{G}}(v'c'\mathbf{k}')\times\sum_{vc\mathbf{k}} C_{vc\mathbf{k}}\rho^{*}_{\mathbf{G}}(vc\mathbf{k})\right\}|v'c'\mathbf{k}'\rangle_{\mathbf{q}}, \quad (12)$$

where $\mathbf{G}$ is a reciprocal-lattice vector, and we have

$$\rho_{\mathbf{G}}(vc\mathbf{k})=\sum_{\mathbf{G}'} u^{*}_{c,\mathbf{k}+\mathbf{q}}(\mathbf{G}')u_{v,\mathbf{k}}(\mathbf{G}'-\mathbf{G}).$$

The term $\mathbf{G}=0$ is included in $\hat{V}_x$ but not in $\tilde{V}_x$.

The efficient computation of the direct part of the electron-hole interaction part of the Hamiltonian requires transformation between different types of representations of the electron-hole pair wave function:

$$\{|vc\mathbf{k}\rangle_{\mathbf{q}}\}\overset{ST}{\Leftrightarrow}\{|\mathbf{x},\mathbf{y},\mathbf{k}\rangle_{\mathbf{q}}\}\overset{FFT}{\Leftrightarrow}\{|\mathbf{x},\mathbf{y},\mathbf{R}\rangle_{\mathbf{q}}\},$$

because $\hat{V}_d$ is most easily handled in the real space, where it is diagonal

$$\hat{V}_d|\mathbf{x},\mathbf{y},\mathbf{R}\rangle_{\mathbf{q}}=-W(\mathbf{x}+\mathbf{R},\mathbf{y})|\mathbf{x},\mathbf{y},\mathbf{R}\rangle_{\mathbf{q}}.$$

Here two types of transformations are indicated by text over the arrows. The transformation from single-particle basis $|vc\mathbf{k}\rangle_{\mathbf{q}}$ to a mixed representation $|\mathbf{x},\mathbf{y},\mathbf{k}\rangle_{\mathbf{q}}$ is a similarity transformation. To transform from the mixed representation to a fully real-space representation $|\mathbf{x},\mathbf{y},\mathbf{R}\rangle_{\mathbf{q}}$, we use fast Fourier transform techniques (FFT). Here $\mathbf{x}$ and $\mathbf{y}$ are hole and electron coordinates within unit cells, and $\mathbf{R}$ is the lattice vector that connects these two cells. $\mathbf{R}$ and $\mathbf{k}$ are FFT conjugated variables. After operating on a state, returning to the single-particle wave-function representation is done by first applying an inverse FFT and then the inverse of the $\{|vc\mathbf{k}\rangle_{\mathbf{q}}\}\Leftrightarrow\{|\mathbf{x},\mathbf{y},\mathbf{k}\rangle_{\mathbf{q}}\}$ transformation. More details about how these transformations can be implemented are found in Ref. 6. The $W(\mathbf{x}+\mathbf{R},\mathbf{y})$ is the screened Coulomb interaction calculated using the Levine-Louie-Hybertsen[12] model for the solid-state screening. In this model, the solid-state screening is calculated using the LDA charge density and the macroscopic dielectric constant ε_∞. The screening is static, and in principle it should be dynamical with structure around the plasma frequency. For many solids, static screening has been found to be adequate.

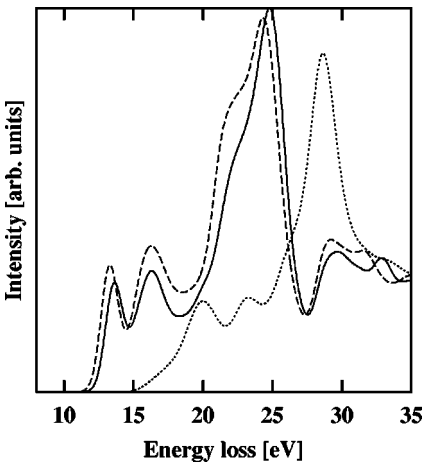

FIG. 1. Theoretical IXS spectrum for LiF within different approximations. The momentum transfer is $1.12\,\text{Å}^{-1}(\approx 0.72\Gamma X)$ along the Cartesian (100) direction. The result neglecting $\hat{V}_d$ is given by the dotted line, and the dashed line is the result when $\tilde{V}_x$ is neglected. The full calculation is given by the solid line.

IV. RESULTS AND DISCUSSION

Because traditional approaches to IXS neglect the direct part of the electron-hole interaction, or it is approximated by introducing ''local-field factor'' $G(\mathbf{q})$,[13] we now note the effects of the electron-hole interaction for insulating and semiconducting materials. The direct part of the interaction is generally equal or larger in magnitude than the exchange part $\tilde{V}_x$. The importance of this interaction in the IXS spectra can be seen in Fig. 1. In the figure, we show a LiF spectrum for momentum transfer $0.72\Gamma X$ with and without including $\tilde{V}_x$ and $\hat{V}_d$. By comparing the full calculation and the calculation neglecting the exchange interaction $\tilde{V}_x$, we see that in comparison to $\hat{V}_d$ the exchange interaction modifies the spectrum only slightly, which is the typical situation for insulators. Neglecting the direct part of the interaction produces much larger changes in the spectrum. The features are shifted by as much as 5 eV to higher energies when neglecting $\hat{V}_d$. Also, the shapes and relative intensities of the features are strongly modified. The sharp exciton peak around 14 eV is absent in calculations without the direct part of the electron-hole interaction. The relative importance of these interactions depends on the material, and it is important that both of these interactions are taken into account in this paper. In particular, the term $(4\pi/q^2)\hat{\rho}^{\dagger}_{\mathbf{q}}\hat{\rho}_{\mathbf{q}}$ is in effect reintroduced when computing $S(\mathbf{q},\omega)$ and this term leads to the

plasmon peak structure that characterizes $S(\mathbf{q},\omega)$ or $\mathrm{Im}[1/\varepsilon_M(\mathbf{q},\omega)]$ for many solids. This means that this part of $\hat{V}_x$ is present also in the calculation without $\hat{V}_d$ and $\tilde{V}_x$. We also note that Fleszar *et al.*[13] found the direct part of the interaction to be more important also for aluminum, although they used $G(\mathbf{q})$ to approximate the effect of $\hat{V}_d$.

We would like to address the numerical accuracy of the results for the cases that we present. The convergence of results with respect to **k**-point sampling and the number of Haydock iterations was analyzed. The estimated relative standard uncertainty is about 2% because of the **k**-point sampling and Haydock recursion iterations specified for each case. This uncertainty is mostly due to the finite number of **k** points. The error due to having a finite number of Haydock recursion steps was estimated to be less than 0.1%.

For the results presented, the dynamic structure factor is shown up to frequencies larger than the ''plasmon peak'' only in LiF. For other systems, we desired to emphasize the near-edge portions of the spectra, which are closely related to interband transitions and associated transition matrix elements. In particular, we would contrast the qualitative differences between spectra for diamond and GaN, which have Wannier-like excitons and give near-edge features that are reasonably well described even within a noninteracting framework, and the spectra for LiF, which has Frenkel excitons and gives near-edge features that are dominated by an exciton peak. In addition, it would be desirable to extend our treatment so that it could include negative-frequency or ''backwards going'' electron-hole pair states from the beginning of a calculation. At present, their effects are addressed by using the relation,

$$\mathrm{Im}\,\varepsilon_M(\mathbf{q},-\omega) = -\,\mathrm{Im}\,\varepsilon_M(\mathbf{q},\omega) \tag{13}$$

but only after computing $\mathrm{Im}\,\varepsilon_M(\mathbf{q},\omega)$ for $\omega>0$, and Kramers-Kronig analysis to obtain $\mathrm{Re}\,\varepsilon_M(\mathbf{q},\omega)$. Because of this, we would suggest that the ''collective-excitation'' portions of our spectra may be on a somewhat less solid footing than the near-edge portions, and we defer further analysis of the former to future work.

A. LiF

We first discuss LiF, which has a rocksalt structure and the lattice constant was taken to be 4.02 Å. The wave functions were calculated on a $12\times15\times15$ mesh in the first Brillioun zone. (The results were essentially the same as those for more symmetric $12\times12\times12$ mesh. Our finer mesh ensured numerical convergence.) The band gap of the band structure was modified from the LDA value 8.82 eV to the *GW* value of 14.30 eV. The valence bands were stretched by 16% to get the *GW* bandwidths. The dielectric constant for LiF is $\varepsilon_\infty=1.92$. The broadening parameter η was taken to be 0.35 eV to mimic the experimental energy resolution of 0.7 eV. The number of iterations for the Haydock recursion was 300.

Figure 2 compares the experimental results[14,15] and the calculated dynamic structure factor for several lengths of the momentum transfer vector **q** along the Cartesian (100) direction. Throughout this paper standard uncertainties are indicated for experimental results. The exciton peak in the energy-loss spectrum around 14 eV is present in the interacting calculation but not in the calculation without the electron-hole interaction $\tilde{V}_x+\hat{V}_d$. The calculated dispersion of the exciton peak follows the experimental values quite accurately. Figure 3 shows the exciton dispersion predicted by our interacting calculation and results from three different experiments. We tried to model this dispersion by a parabolic function:

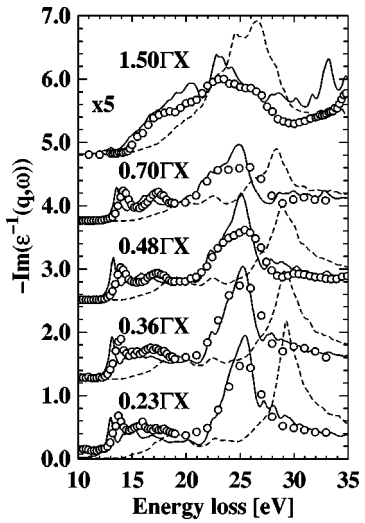

FIG. 2. IXS spectra of LiF as a function of momentum transfer along ΓX. The solid lines are the spectra calculated including the electron-hole interaction, and broken lines without the interaction. Experimental data are given by the circles, and the experimental standard uncertainty is smaller than the symbol size. The spectra for $q=0.23\Gamma X$ and $0.36\Gamma X$ are multiplied by 3 because of their lower intensity.

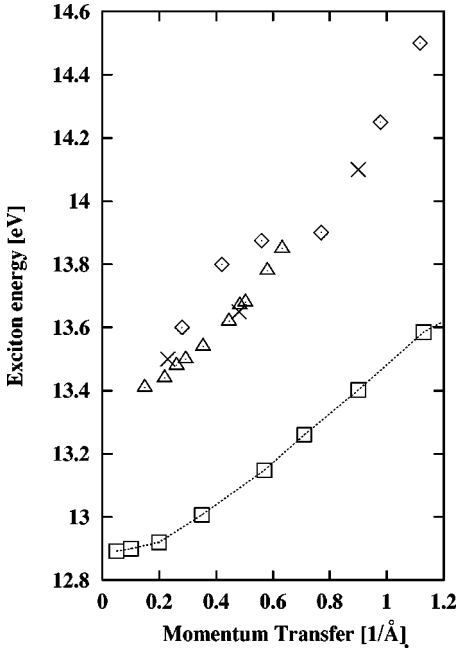

FIG. 3. The dispersion of the exciton peak position as a function of momentum transfer along the Cartesian (100) direction. The three experimental results are given by diamonds (Ref. 14), by triangles (Ref. 16), and by the crosses that indicate our interpretation of Fig. 3 in Ref. 17. The theoretical result is given by the squares, and the line is only shown to guide the eye.

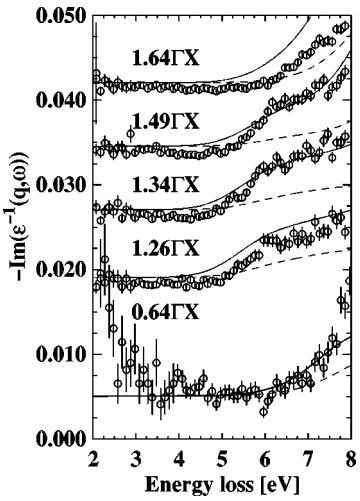

FIG. 4. Calculated and experimental IXS spectra for diamond. The data are given near the band gap as a function of momentum transfer along the ΓX direction. The experiment is given by the open circles, the IXS spectra including the electron-hole interaction by the solid line, and the theory neglecting electron-hole interaction by the dashed line.

$$\omega_{est} = \omega_0 + q^2/2M.$$

Here ω_{est} is the estimated energy of the exciton, ω_0 is a constant energy shift because of the band gap and the exciton binding energy, and M is the effective mass of the exciton. There is an approximately 0.6 eV discrepancy in the position ω_0 between theory and experiment. We calculated the theoretical exciton energy for several momentum transfers from $0.05\,\text{Å}^{-1}$ up to over $1.0\,\text{Å}^{-1}$. The effective mass we obtained this way changes depending on the momentum transfer points we take into account, which indicates nonparabolicity. For the momentum transfers given in Fig. 2 this value is as much as eight times the mass of the electron (m_e) for both the experiment and the theory. For momentum transfers under $0.4\,\text{Å}^{-1}$ we obtain the value $M = 3.9m_e$ which is closer to the value of $3.3m_e$ given in Ref. 16. This would suggest that the LiF exciton does not follow simple parabolic dispersion. The other features of the spectrum are quite well reproduced by the calculations.

B. Diamond

The single-particle wave functions and the LDA band energies for diamond were calculated using the experimental lattice constant of 3.57 Å. The indirect band gap of diamond was changed from the LDA value of 3.90 eV to the 5.5 eV obtained from *GW* calculation. The LDA valence bands were stretched 7%. The value of ε_∞ is 5.5 for diamond. A mesh of $16\times16\times16$ **k** points in the first Brillioun was used for calculating the single-particle wave functions and 300 Haydock recursion iterations were used.

The results for diamond can be seen in Fig. 4. Again, the result is given for several values of **q** along the (100) Cartesian direction. The agreement between experiment[14,15] and theory is poorer in this case than for LiF. The value of the indirect band gap (around 5.5 eV) is approximately the same both in experiment and theory. The indirect band gap is approximately measured when the momentum transfer extends from the Γ point to the second Brillouin zone ($1.35\Gamma X$) but not when it is in the first Brillouin zone ($0.64\Gamma X$). We note that there is a difference between the actual momentum of the minimal band gap ($0.75\Gamma X$ or $1.25\Gamma X$) and the momentum values considered in this work ($0.64\Gamma X$ or $1.35\Gamma X$). We have considered the latter values, because these momenta were selected in measurements. However, the effects of using slightly different momenta are quite minor in this case. The momenta chosen are near the actual conduction-band minimum (CBM), the conduction bands are quite flat near the CBM, and the ''selection rule'' (discussed below) that renders the gap unobserved in the first Brillouin zone applies equally well along an extended portion of the Δ line. The Brillouin-zone ''selection rule'' can be explained using symmetry arguments. The principles of these arguments can be correctly applied even in a single-particle picture, in which they involve the symmetries of the Bloch states in question. The valence-band maximum (VBM) is at the Γ, and the CBM is at approximately $0.75\Gamma X$. The valence-band state near Γ written as a linear combination of atomic orbitals is

$$|\psi_{n\mathbf{k}}(\text{VBM})\rangle \sim |2p_\alpha,\tau_1\rangle - |2p_\alpha,\tau_2\rangle.$$

The index α indicates a Cartesian coordinate, and $|2s,\tau\rangle$ and $|2p_\alpha,\tau\rangle$ are atomic states on one of the two sites τ in the unit cell. Near the CBM, the Bloch states have the form

$$|\psi_{n\mathbf{k}'}(\text{CBM})\rangle \sim \sum_\tau e^{i\mathbf{k}'\cdot\tau}[A(\mathbf{k}')|2s,\tau\rangle + B(\mathbf{k}')|2p_\alpha,\tau\rangle],$$

where α is the Cartesian direction of the Δ line parallel to **q**. Analogous orbitals on equivalent sites are combined with opposite signs at VBM and indicated phases at the CBM. Combining these equations we can calculate the transition matrix element

$$\begin{aligned}\langle\psi_{n\mathbf{k}'}(\text{CBM})|e^{i\mathbf{q}\cdot\hat{\mathbf{r}}}|\psi_{n\mathbf{k}}(\text{VBM})\rangle &\sim (e^{i(\mathbf{q}-\mathbf{k}')\cdot\tau_1} - e^{i(\mathbf{q}-\mathbf{k}')\cdot\tau_2})[A(\mathbf{k}')\langle 2s|e^{i\mathbf{q}\cdot\hat{\mathbf{r}}}|2p_\alpha\rangle \\ &\quad + B(\mathbf{k}')\langle 2p_\alpha|e^{i\mathbf{q}\cdot\hat{\mathbf{r}}}|2p_\alpha\rangle],\end{aligned} \tag{14}$$

where $\hat{\mathbf{r}}$ is the position operator and we have neglected the matrix elements between different sites. With $\mathbf{k}\approx0$ and **q** in the first Brillouin zone, for which we have $\mathbf{q}=\mathbf{k}'\approx0.75X$, the first factor of the matrix element is zero. However, with **q** in the second Brillouin zone we have $\mathbf{q}=\mathbf{k}'+\mathbf{G}$, where **G** is the reciprocal-lattice vector at $2X$, and we have constructive interference between the matrix elements at different atomic sites. In this way the CBM states at $\mathbf{k}'\approx-0.75X$ are probed. Further comparison of results is given in Ref. 15.

In many-body calculations such as the ones we have done, the analysis of the results is much more difficult than in the case of one-particle calculations. It is possible however to do a spectral decomposition to the system, as was explained in Ref. 6. The idea is to find the solution $|\Phi(\mathbf{q},\omega)\rangle$ to the equation

$$(\omega - H_{eff} + i\eta)|\Phi(\mathbf{q},\omega)\rangle = 2\sqrt{\pi\eta}\rho_{\mathbf{q}}^\dagger|0\rangle \tag{15}$$

for a given momentum and energy transfer. Then the imaginary part of dielectric function ε_M can be obtained by

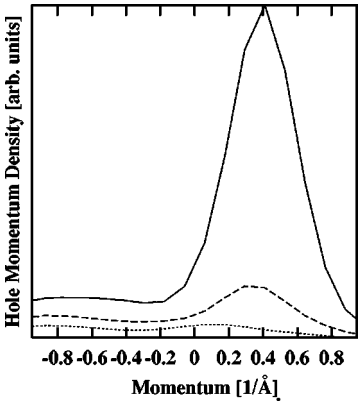

FIG. 5. The hole momentum density in diamond averaged over the $k_y k_z$ plane. The magnitude of the momentum transfer is $1.13\,\text{Å}^{-1}(\approx 0.65\Gamma X)$, and its direction is the Cartesian (100) direction. The figure shows the momentum density for three different values of energy transfer ω. The dotted line is for $(\omega=)6$ eV, the dashed line is for 7 eV, and the solid line is for 8 eV.

$$\text{Im}\,\varepsilon_M(\mathbf{q},\omega) = 1/q^2 \sum_{vc\mathbf{k}} |_{\mathbf{q}}\langle vc\mathbf{k}|\Phi(\mathbf{q},\omega)\rangle|^2. \qquad (16)$$

Because structure in $S(\mathbf{q},\omega)$ comes mainly from $\text{Im}\,\varepsilon_M$ this gives us an opportunity to study more closely what bands and portions of the first Brillouin zone contribute to an IXS spectrum. To do this, one may plot the projection of $|\Phi(\mathbf{q},\omega)\rangle$ onto $|vc\mathbf{k}\rangle_{\mathbf{q}}$ states as a function of energy ω and some momentum ($\mathbf{k}$) component while averaging over other momentum components and single-particle states (v,c).

Figures 5 and 6 show one way to depict this result. The figures show, for selected energy transfers, the hole momentum distribution averaged over possible electron-hole states and two Cartesian components of the hole momentum. Note that in Figs. 5 and 6 the average is taken over the yz plane that is perpendicular to the scattering vector. The analogous result for the average over the xz plane shows that for both momentum transfer values and all the values of energy transfer, the hole momentum is centered around $k_y=0$. By symmetry this implies, as expected, that the hole momentum is primarily near the x axis Δ line (Γ-X). The position and shape of the main peak of the distribution depends both on the momentum and the energy transfer. By averaging instead

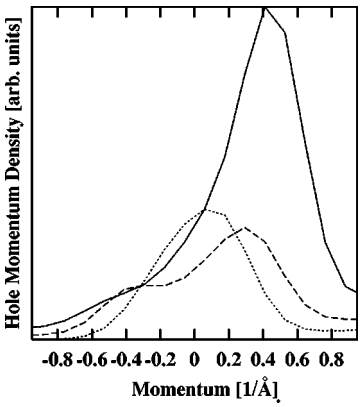

FIG. 6. Same as in Fig. 5, but for momentum transfer $2.36\,\text{Å}^{-1}(\approx 1.35\Gamma X)$.

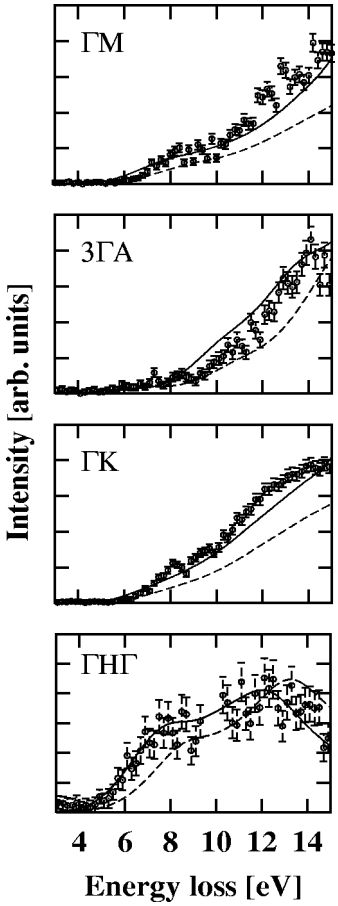

FIG. 7. Theoretical and experimental IXS spectra of wurtzite GaN for several different momentum transfers. An experimental spectrum (Ref. 18) is presented with open circles and the error bars indicate the experimental uncertainty. Theory including the electron-hole interaction is given by the solid line. The direction and magnitude of the momentum transfer is indicated.

over all the hole momentum components for given electron-hole pair states (c,v) we can conclude that for $\omega=8$ eV and $\mathbf{q}=0.65\Gamma X$ the scattering strongly involves excitations from the highest valence-band state with crystal momentum $\approx 0.22\Gamma X$ to the second lowest conduction band with crystal momentum $\approx 0.87\Gamma X$. For the momentum transfer $\mathbf{q}=1.35\Gamma X$, the loss function has significant weight at $\omega \approx 6$ eV, and the dominant excitation is from valence-band states near Γ to the lowest conduction band state around $1.35\Gamma X$. This shows that the spectral features around 5.5 eV are simply measuring transitions across the indirect band gap of diamond and that these features are not qualitatively changed by the electron-hole interaction.

C. Wurtzite GaN

Wurtzite GaN was studied with lattice constants taken to be $a=3.189$ Å and $c=5.185$ Å. The internal parameter was set to $u=0.377$. The band gap was taken as the *GW* 3.5 eV (the LDA result is 2.3 eV), and the valence bands were stretched by 8%. A grid of $16\times16\times16$ $\mathbf{k}$ points in the first Brillouin was used for calculating single-particle wave functions. The value for the dielectric constant ε_∞ was 5.5 and number of iterations in Haydock recursion was 300.

In Fig. 7 theoretical spectra are compared with experimental[18] ones for several different values of momentum. Agreement between theory and experiment is quite good. Two features for the case with momentum transfer $\Gamma H\Gamma$ are quite well reproduced both in relative intensity and position. The other three spectra are also quite well reproduced. In the $\mathbf{q}=3\Gamma A$ case, there is clear dip around 14 to 15 eV in the experimental data and this is also present in the theory, although its strength is underestimated. There is a plateau from 8 to 10 eV in the experimental data for the momentum transfer of ΓM. Again this feature is much smoother in the theoretical spectrum.

V. CONCLUSION

We have presented a first-principles scheme for calculating the dynamic structure factor $S(\mathbf{q},\omega)$ of crystalline insulators and semiconductors. The method was applied to LiF, diamond, and wurtzite GaN for several different momentum transfers. Agreement with experiment was found to be very good. The inclusion of the electron-hole interaction in the description of inelastic scattering was found to be essential. The electron-hole interaction redistributes spectral weight compared to noninteracting calculations. Without the interaction, many of the features of the spectrum such as exciton peaks would not be present at all.

ACKNOWLEDGMENTS

We would like to acknowledge W. A. Caliebe, C.-C. Kao, and K. Hämäläinen for providing us with the experimental data for LiF and diamond. Additionally we would like to thank W. A. Caliebe for his guidance at various points in the work. We would especially like to acknowledge S. Huotari, K. Hämäläinen, C.-C. Kao, and S. Manninen for letting us use their experimental results for GaN prior to publication. The experimental work on GaN was done at beamline X21 at the National Synchrotron Light Source, Brookhaven National Laboratory. J.A.S. is supported by the Finnish Academy of Science and Letters.

[1] P. Hohenberg and W. Kohn, Phys. Rev. **136**, 864 (1964); W. Kohn and L. J. Sham, Phys. Rev. **140**, 1133 (1965).
[2] L. Hedin, Phys. Rev. **139**, 796 (1965).
[3] M. S. Hybertsen and S. G. Louie, Phys. Rev. Lett. **55**, 1418 (1985); Phys. Rev. B **34**, 5390 (1986); E. L. Shirley, L. J. Terminello, J. E. Klepeis, and F. J. Himpsel, *ibid.* **53**, 10 296 (1996).
[4] B. C. Larson, J. Z. Tischler, E. D. Isaacs, P. Zschack, A. Fleszar, and A. G. Eguiluz, Phys. Rev. Lett. **77**, 1346 (1996); W. Schülke, K. Höppner, and A. Kaprolat, Phys. Rev. B **54**, 17 464 (1996); J. P. Hill, C.-C. Kao, W. A. Caliebe, D. Gibbs, and J. B. Hastings, Phys. Rev. Lett. **77**, 3665 (1996).
[5] N. E. Maddocks, R. W. Godby, and R. J. Needs, Phys. Rev. B **49**, 8502 (1994); A. Fleszar, A. A. Quong, and A. G. Eguiluz, Phys. Rev. Lett. **74**, 590 (1995); H. Bross and M. Ehrnsperger, Z. Phys. B: Condens. Matter **97**, 17 (1995).
[6] L. X. Benedict and E. L. Shirley, Phys. Rev. B **59**, 5441 (1999).
[7] See, for example, A. Fetter and J. D. Walecka, *Quantum Theory of Many-Particle Systems* (McGraw-Hill, San Francisco, 1971), pp. 538–539.
[8] L. X. Benedict, E. L. Shirley, and R. B. Bohn, Phys. Rev. B **57**, R9385 (1998); Phys. Rev. Lett. **80**, 4514 (1998).
[9] For a review, see W. E. Pickett, Comput. Phys. Rep. **9**, 115 (1989).
[10] E. L. Shirley, Phys. Rev. B **54**, 16 464 (1996).
[11] R. Haydock, Comput. Phys. Commun. **20**, 11 (1980).
[12] Z. H. Levine and S. G. Louie, Phys. Rev. B **25**, 6310 (1982); M. S. Hybertsen and S. G. Louie, *ibid.* **37**, 2733 (1988).
[13] See, for example, A. Fleszar, A. A. Quong, and A. G. Eguiluz, Phys. Rev. Lett. **74**, 590 (1995).
[14] W. A. Caliebe, Ph.D. thesis, University of Kiel, 1997.
[15] W. A. Caliebe, J. A. Soininen, E. L. Shirley, C.-C. Kao, and K. Hämäläinen, Phys. Rev. Lett. **84**, 3907 (2000).
[16] A. A. Cafolla, Ph.D. thesis, University of Virginia, 1985.
[17] J. R. Fields, P. C. Gibbons, and S. E. Schnatterly, Phys. Rev. Lett. **38**, 430 (1977).
[18] S. Huotari, K. Hämäläinen, C.-C. Kao, and S. Manninen (unpublished).